Contents

List of Figures

Acronyms

This document is incomplete. The external file associated with the glossary 'acronym' (which should be called `main_phd.acr`) hasn't been created.

Check the contents of the file `main_phd.acn`. If it's empty, that means you haven't indexed any of your entries in this glossary (using commands like `\gls` or `\glsadd`) so this list can't be generated. If the file isn't empty, the document build process hasn't been completed.

Try one of the following:

- Add `automake` to your package option list when you load `glossaries-extra.sty`. For example:
  `\usepackage[automake]{glossaries-extra}`
- Run the external (Lua) application:
  `makeglossaries-lite.lua "main_phd"`
- Run the external (Perl) application:
  `makeglossaries "main_phd"`

Then rerun LaTeX on this document.

This message will be removed once the problem has been fixed.

Chapter 1
Evaluation of the Light Propagation Model in the Near Infrared

Abstract Imaging in deep tissue without optical clearing usually occurs in the diffusion domain, however, there are reasons that point to consider near infrared (NIR) windows as low scattering media. This chapter reviews the optical properties of tissues for NIR light and evaluates the validity of the Diffusion Approximation (DA) for such regime using a novel MC method.

1.1 Validity Conditions of the Diffusion Approximation

Light propagation in highly scattering media is governed by the laws of the diffusion phenomena. At a few μm from the source light loses its directionality, propagating isotropically no matter the initial emission pattern. General electromagnetic transport problems can be accurately modeled through the Radiative Transport Equation (RTE) [1], an expression closely related to the equation of energy conservation capable of predicting the exchange of energy due to absorption and scattering interactions—among others—within small differential volumes in space and time. As this equation usually lacks of an analytical solution, approximations are taken in order to find an expression to calculate the intensity and the flux at a certain point in space and time. This is the case of the DA, an equation derived from the RTE that models light propagation as a gradient of concentration of optical energy. Light diffuses from regions of more concentration to those of less following Ficks's laws of diffusion and Fourier's for heat transport [1, 2].

The approximations introduced for the derivation of the DA—more details can be found in chapter **??**, and in specialized literature [1–3]—allow to obtain a solution that provides very accurate results far from the source in strongly scattering media but constraints its use for this particular case. More specifically, the expression for the diffuse intensity $I_d(\mathbf{r}, \hat{\mathbf{s}})$, also named as the angular distribution of diffuse light, restricts the validity of the solution for regions close to the source. The DA defines the $I_d(\mathbf{r}, \hat{\mathbf{s}})$ as the result of a weighted sum of two contributions: the average diffuse intensity $U_d(\mathbf{r})$, which yields a uniform intensity, and the diffuse flux density $\mathrm{J}_d(\mathbf{r})$, which gives some directionality. The use of this

expression is usually named as the P_1 approximation and is derived through a first order spherical harmonic expansion as was described in equation **??**.

The angular distribution from the diffuse intensity is accurate to describe the intensity when the initial directionality of light is completely lost and the radiance has no preferential direction of propagation. This is the general case for point sources at a distances of approximately one l_{tr}^{*} [4], and for collimated sources when the intensity and flow of energy can be modeled as that of an equivalent point source [2, 5]. In chapter **??**, figure **??** illustrated this equivalence using the $U(\mathbf{r})$ derived from MC simulations [6], showing how the propagation far from sources can be modeled with the same function no matter the initial shape or directionality of light.

The higher contribution of the ballistic components of light—$U_{ri}(\mathbf{r})$ and $\mathrm{J}_{ri}(\mathbf{r})$—at distances from the source below l_{tr}^{*} is the main cause for the failure of the DA [7]. Despite in this region the intensity in the direction of propagation is usually assumed to decay according to the Beer-Lambert (B-L) law, the effect of scattered light in the ballistic to diffusion transition is yet not fully understood. Studies have shown that the DA is accurate from distances that range from one to several transport mean free paths [8, 9]; however, how the spatial distribution of the intensity—specially for collimated sources—changes at short distances or in low scattering media is still unknown. Some works have attempted to improve the accuracy of the DA at short l_{tr}^{*} distances using higher orders of spherical harmonic expansions to model $I_d(\mathbf{r}, \hat{\mathrm{s}})$, named P_N approximations [**Star1989**]. Others, have stepped back to the RTE to use hybrid RTE-DA models to describe accurately light in the proximity to sources or in low scattering regions [10]. Most of these approaches use MC simulations as the gold standard to validate the results. Moreover, since this method used to be computationally expensive, some hybrid methods have been suggested in which MC was used to complement the inaccuracies of the DA at short distances [11].

Summarizing, the DA can be considered adequate to model light propagation in high scattering media, where the l_{tr}^{*} distance is very short and thus most of the measurements are performed far from the sources in the diffusion domain.

1.2 Propagation Regime of Light in the Near Infrared Window

Chapter **??** of this thesis gave an overview of the optical properties of some biological tissues for NIR light. The most remarkable change respect to the visible region is the abrupt reduction of the scattering coefficient μ_s'. The use of longer wavelengths increases the ratio of λ respect to the size of scatterers of the medium which, given the Mie theory [12], increments the scattering anisotropy. In general, the reduction of μ_s' in the NIR can be modeled with an inverse power law [13], therefore it is easy to extrapolate its magnitude from its values in the visible region if these are well characterized and studied. The change

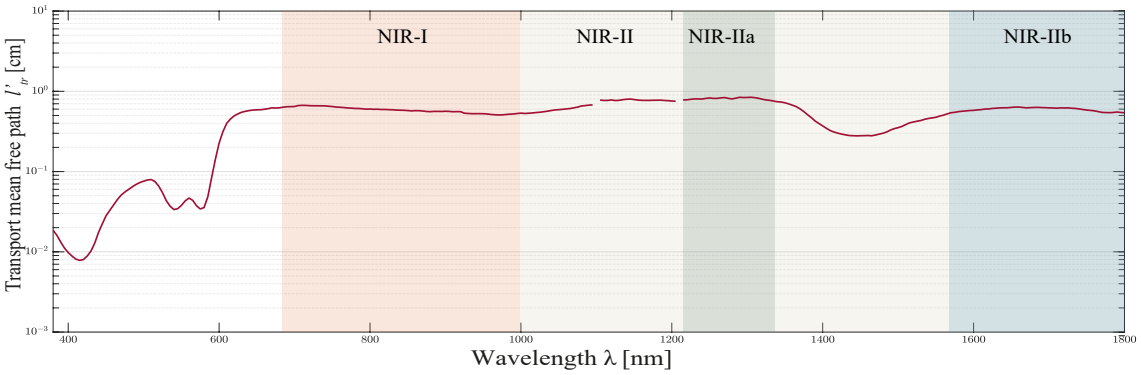

Figure 1.1 Transport mean free path for blood 98% oxygenated blood. Data extracted from [14].

in the absorption coefficient μ_a throughout the spectrum is less deterministic since it has high dependency on the chromophores of the tissue.

In order to understand what can be expected when imaging in the NIR and why, we must take a look back at the values of the optical properties of tissues. As can be deduced from the previous section of this chapter, by looking at the transport mean free path l^*_{tr} the propagation regime of light can be determined, predicting whether the measurements will occur in the diffusion domain or not. This coefficient indicates the depths at which the DA starts to hold, given the assumptions taken during its derivation. Figure 1.1 shows the l^*_{tr} for 98% oxygenated blood, where it can be clearly seen that the the distances under which the diffusion model should not be valid are significantly longer in the NIR region, reaching values of up to 1 cm in the second near infrared (NIR-II) window. It is important at this point to underline that this values are equivalent to light penetrating into tissue with all the chromophores of the blood still intact, as occurs during *in vivo* imaging. In a similar way, figure 1.2 shows the transport mean free path for skin and subcutaneous adipose tissue, two of the most attenuating and scattering tissues. The literature of optical properties often lacks of values for the NIR window, specially the NIR-II. To give a better understanding of the scenario in the NIR-II, figure 1.3 shows the scattering coefficients for skin, brain, skull and soft tissue. In general, all of them show either an increment of the transport mean free path or a significant decrease of the scattering coefficient in the NIR.

Moreover, as was described in chapters **??** and **??**, imaging techniques such as Light Sheet Fluorescence Microscopy (LSFM) or Optical Projection Tomography (OPT) rely on low scattering media or very short propagation paths of light to achieve high resolution images. This scenario can be found in small sized specimens and in optically transparent samples. Large and highly scattering pieces of tissue can undergo optical clearing, which reduces significantly μ'_s and increases the anisotropy of the medium [16], homogenizing the index of refraction of and increasing the transmittance [17]. The evaluation of the μ'_s value after tissue clearing has been studied in some works, reporting ratios of reduction, named as optical clearing potential (OCP) [18], that range from three to eightfold depending on the clearing agent and the duration of the protocol [19–21].

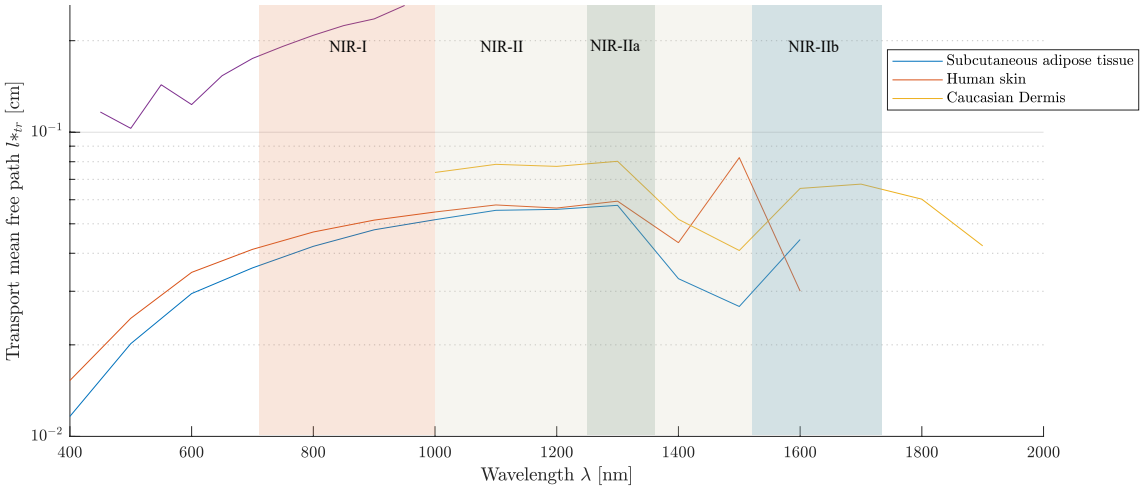

Figure 1.2 Transport mean free paths for human tissue, adipose tissue and muscle. Data extracted from [15].

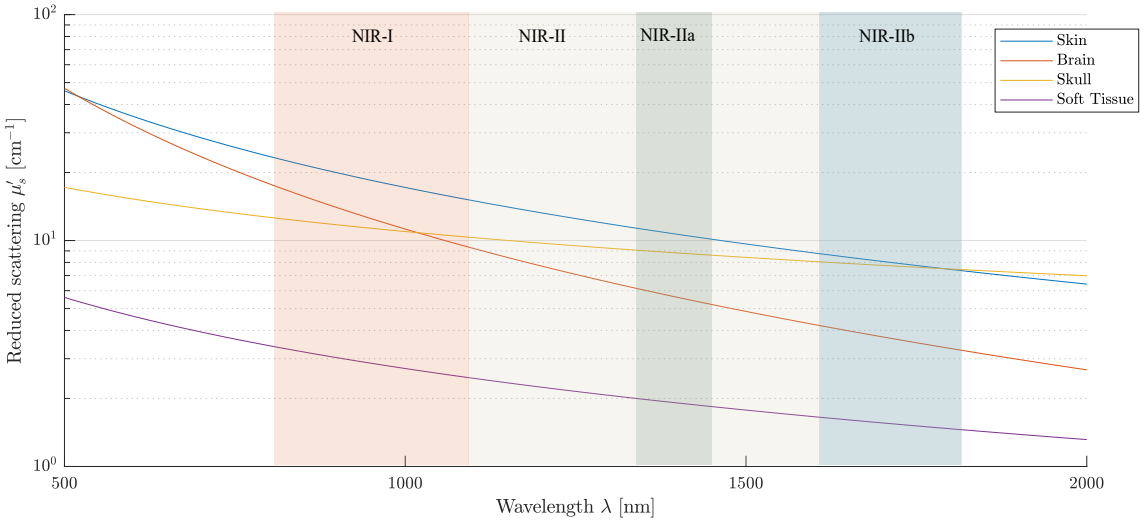

Figure 1.3 Scattering coefficient for several biological tissues. Data extracted from [13].

Considering the optical properties of tissues in the NIR and taking into account the additional reduction of μ_s' we can clearly see thatmost common optical microscopy and mesoscopy modalities measure below the diffusion barrier. In fact, the NIR-II has already been proved to have the best penetration depths of the spectrum [22]. Under extremely low scattering or very short distances, the Beer-Lambert equation (see equation **??**) should be enough to model light attenuation, however, as was explained in chapter **??**, scattering is still present and affecting the imaging process.

Thus, the measurements in these techniques fall in the yet undetermined ballistic to diffusion transition. The intermediate regime where neither B-L or the DA can model accurately the propagation of light and therefore methods to introduce compensations for the effects of scattering are missing.

In this chapter we aim to find a reliable method to study light propagation in the transition from the ballistic to the diffusion domain taking in consideration the particularities

of imaging systems and the way they measure optical quantities in order to enable future developments of method to revert the negative effects of scattering on images.

1.3 Analytical Expressions for the Flux Density in the Diffusion Approximation

In order to compare the results of the simulator with the diffusion theory, the equations that describe the flux in the ballistic and the diffuse domain are presented in this section.

The measured power in a detector P_{det}, as shown in equation1.1, can be expressed as the total flux density $\mathrm{J}(\mathbf{r})$ that flows in the normal direction respect to the surface of the sensor $\hat{\mathrm{n}}$, integrated over its area $\mathrm{d}S$ [2].

$$P_{det} = \int_A \mathrm{J}(\mathbf{r}) \cdot \hat{\mathbf{n}} \mathrm{d}S, \qquad [\mathrm{W}] \tag{1.1}$$

The the flux density $\mathrm{J}(\mathbf{r})$ is related to the specific intensity $I(\mathbf{r}, \hat{\mathrm{s}})$ through equation 1.2.

$$\mathrm{J}(\mathbf{r}) = \int_{(4\pi)} I(\mathbf{r}, \hat{\mathrm{s}}) \hat{\mathrm{s}} \mathrm{d}\Omega \qquad [\mathrm{W/cm^2}] \tag{1.2}$$

It is important to note from the expressions of $I(\mathbf{r}, \hat{\mathrm{s}})$ and $\mathrm{J}(\mathbf{r})$ that the flux takes into account the directional component, normally computed as a directional cosine, and thus it has a vectorial nature. The detected quantity in MC simulators, $U(\mathbf{r})$, does not discriminate the propagation direction of the $I(\mathbf{r}, \hat{\mathrm{s}})$, contributing all directions equally to its magnitude, as shown in 1.3.

$$U(\mathbf{r}) = \int_{(4\pi)} I(\mathbf{r}, \hat{\mathrm{s}}) \mathrm{d}\Omega \qquad [\mathrm{W/cm^2}] \tag{1.3}$$

Depending on the propagation regime, the equation for the flux is expected to have different expressions that can be distinguished as the reduced $\mathrm{J}_{ri}(\mathbf{r})$ and the diffuse $\mathrm{J}_d(\mathbf{r})$ components. We present below the analytical solutions for a point source and a collimated pencil beam source in both regimes.

Point Source

In diffusive media, the flux can be calculated directly from Fick's law with equation 1.4. Being D the diffusion coefficient presented in chapter **??**, equation **??**.

$$\mathrm{J}_d(\mathbf{r}) = -\mathrm{D} \nabla U_d(\mathbf{r}) \qquad [\mathrm{W/cm^2}] \tag{1.4}$$

The z component of the 3D gradient corresponds to the flux in the forward direction, therefore the expression of $\mathrm{J}_d(\mathbf{r})$ can be written as in equation 1.5. This is the expression

that will be used throughout the comparisons against the MC simulations for a point source in this chapter.

$$\mathrm{J}_d(\mathbf{r}) = -\mathrm{D}\frac{\partial U_d(\mathbf{r})}{\partial z} \qquad [\mathrm{W/cm^2}] \tag{1.5}$$

As a reminder, the diffuse intensity $U_d(\mathbf{r})$ corresponds to the convolution of the point source profile with the Green's function presented in chapter **??**, equation **??**. For convenience, this expression is rewritten below.

$$U(\mathbf{r}) = S_0\frac{\exp\left(ik_0\mathbf{r}\right)}{4\pi D\mathbf{r}}$$

Collimated Pencil Source

Collimated sources have a highly directional component near the source. Below l_{tr}^* the flux can be estimated through the reduced component $\mathrm{J}_{ri}(\mathbf{r})$ from the expression of the B-L law intensity, $I_{ri}(\mathbf{r}, \hat{\mathbf{s}})$, shown in eq. 1.6

$$I(\mathbf{r}, \hat{\mathbf{s}}) = S_0\delta(\mathbf{R} - \mathbf{R}_s)\exp\left(-\mu_{tr}z\right)\delta(\hat{\mathbf{s}} - \mathbf{u}_z), \quad \forall \quad z \geq 0 \tag{1.6}$$

Taking into account the property of the delta function of equation 1.7, the reduced flux for a collimated pencil beam close to the source and along the propagation direction is equal to the B-L intensity, decaying according to μ_{tr}.

$$\int_{(4\pi)} \delta(\hat{\mathbf{s}} - \hat{\mathbf{s}}')\mathrm{d}\Omega = 1 \tag{1.7}$$

In diffusive media, the flux should be equivalent to that of a point source after propagating one l_{tr}^* [2, 3]. This two models lead to an undetermined transition expression where the flux should be model as a combination of $\mathrm{J}_{ri}(\mathbf{r})$ and $\mathrm{J}_d(\mathbf{r})$.

1.4 Monte Carlo Simulator for the Forward Optical Flux Density

The Monte Carlo methodfor photon transport is the gold standard solution for the RTE [6, 23]. This simulation framework models tissue interactions of single photon packets as probability distributions, describing the propagation of photons through a sequential and cyclic process of movement, absorption and scattering events that is repeated until a termination rule is met. Since this method calculates a statistical approximation to the solution of the RTE, a large number of photons need to launched in order to obtain robust results. Typically, MC simulations require to run at least 10^6 photons, which can be computationally intensive depending on the parameters of the simulation.

The MC method is a well validated computational algorithm for photon propagation that has been widely used in biomedical optics [24], nuclear medicine [25], radiotherapy [26] or diagnostic radiology [27]. Parallel implementations allow to accelerate its execution massively using Graphics Processing Unit (GPU) computing [28, 29], therefore nowadays executions can be run within seconds.

Although the MC method yields very accurate results for the estimation of $U(\mathbf{r})$, in optical systems the measured quantity obtained by a sensor can be described as the amount of energy that traverses its surface, represented by the flux density $\mathrm{J}(\mathbf{r})$ [2]. Conventional MC simulators store the weight of the photon at each scattering interaction in the corresponding voxel position where the event occurs. This approach loses the directional component of the energy flow and diverges from what be expected in a real detector.

Moreover, another problem of the MC method is that the spatial distribution of the accumulated energy is discretized and stored in a grid with a certain finite size. Whereas the size of these bins does not affect the results of the simulations, the fact that the gird has finite dimensions imposes several restrictions to the method. Firstly, the medium is not infinite anymore, as most MC implementations will terminate photons attempting to cross the boundary interfaces. Secondly, due to memory limitations, very fine grids for large 3D volumes cannot be easily handled, specially when running GPU accelerated versions as these devices usually have very limited dedicated memory resources.

In this work we aim to overcome these limitations by reimplementing the detection scheme of a well validated MC code [30] to make it capable of rendering the flux density in a certain direction for true infinite media with nearly unlimited spatial resolution. The results will be compared with that of the diffusion theory to propose a new method to elaborate novel characterizations of light propagation in low scattering media.

1.4.1 Monte Carlo Implementation

The custom MC implementation has to be able to calculate the spatial distribution of the forward flux in an true infinite domain without spatial restrictions. This requirements can be met by introducing the following modifications to the standard MC implementation:

Calculation of the flux:

Since the flux is defined as the intensity traversing an interface, the simulator evaluates the photons crossing a certain number of equidistant z planes introduced as an input parameter. For each of these detection planes, the MC algorithm accumulates the weight of the photons crossing that interface. To compute this, after each photonmovement step the program checks the z detection planes traversed during its traveled path from the previous position to the current. From this trajectory ,the exact spatial coordinates of intersection with each of the crossed z planes can be calculated. The detected energy for each photon at

these spatial positions is calculated as the z component of the weight, which is computed taking into account the directional cosine of the photon in the z direction (see figure 1.4). This particular way of computing the detected energy for each photon is key to obtain the flux in the forward direction, otherwise, the results would be very close to the $U(\mathbf{r})$.

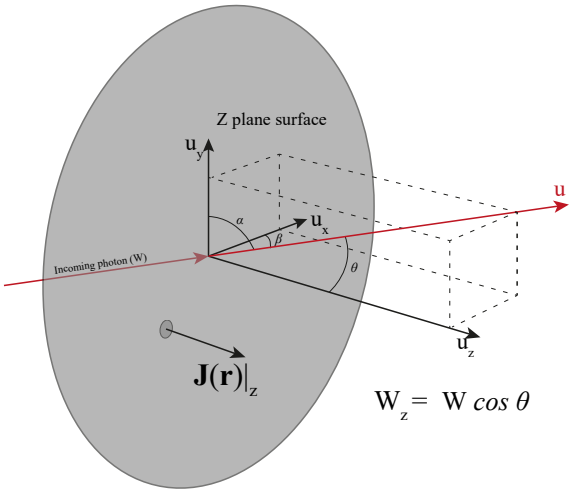

Figure 1.4 Illustration of the detection of a photon. The contribution to the flux for each photon crossing a detection plane is calculated as the z component of its weight using the directional cosines.

Removal of the voxel limitations:

To eliminate any constraint in terms of spatial resolution and range of depths in the simulations, the detected photons are not stored in a 3D grid in cartesian coordinates anymore. Instead, the measured flux is saved in bins arranged in cylindrical coordinates. Exploiting the fact that point and collimated sources in homogeneous media have circular symmetry, the angular component of the polar coordinates for each detection plane can be dropped, saving only the depth and the radial positions of each photon (see figure 1.5). The use of annular detectors reduces the size of the data array in memory from $\mathbb{R}^3$ to $\mathbb{R}^2$. Therefore, now the flux is calculated over a 2D matrix of dimensions NZ and NR with step distances between depth planes and radial bins of dz and dr, respectively.

Moreover, to perform the simulations in a true infinite media, there are no boundaries for the medium, propagating every photon indefinitely until the whole weight has been deposited.

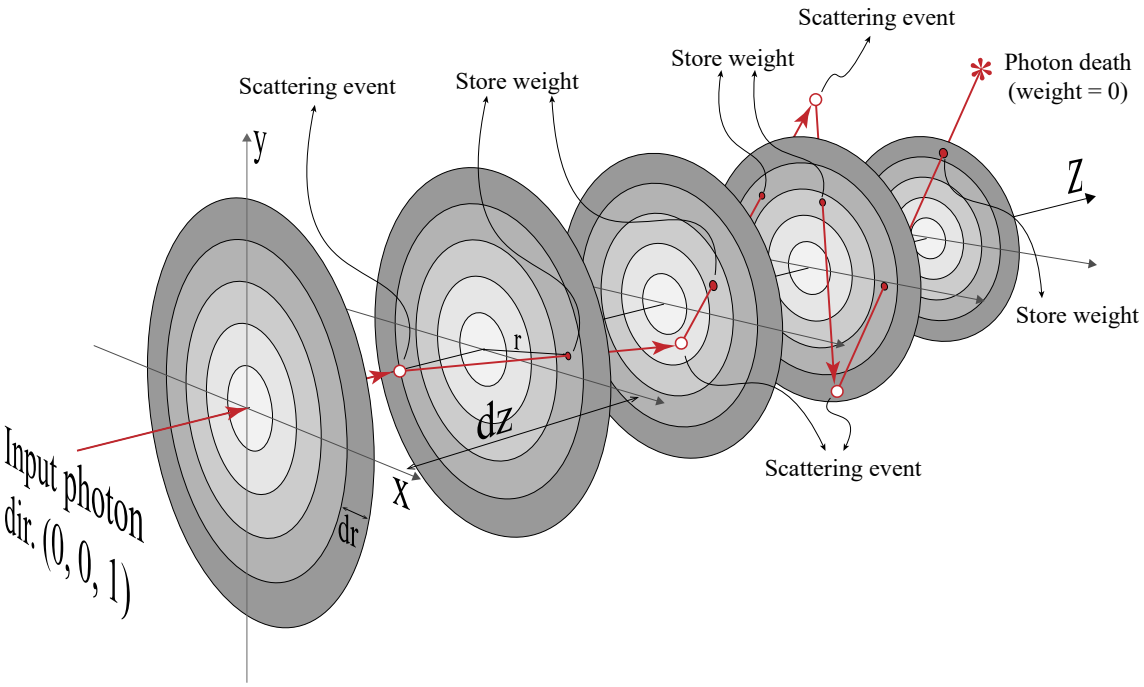

Figure 1.5 Example of the propagation of a photon in the MC flux simulator

Data normalization:

The output data from the MC simulator is normalized for the size of the integration areas. Although the radial step dr is constant, the surface of the bins increases quadratically with the distance from the center, therefore this is taken into account before comparing the results. Additionally, the MC output is also normalized for the number of photons run in the simulation and the 4π factor present in the analytical solution. No additional normalization are introduced to the results.

In this MC implementation is very inexpensive in terms of memory resources however, since each photon propagation is ran until it terminates, there are no chances of stopping them prematurely due to attempting to escape from the volume as occurs in other implementations. This increases the execution time significantly, specially for highly scattering media with poor absorption with a large amount of z positions to evaluate.

For this reason, the simulation was ported into GPU in order to make it more usable and to reduce the execution times. The code was implemented for the Nvidia CUDA platform, showing a reduction of the computation time of 10x-100x depending on the simulation parameters.

1.4.2 Monte Carlo Code Validation

The results of the MC code were validated with simulations of a diffusion scenario where the flux is well known and characterized by the DA. The results were compared against

the analytical solution of $\mathbf{J}(\mathbf{r})$ for a point source. In order to ensure enough statistical robustness of the simulated data that will be presented from now on, all the cases are run for 10^9 photons.

The DA shows very good agreement with the results of the MC simulations, as can be seen in figure 1.6. Despite there is a small scaling mismatch in the amplitudes, the trends above l^*_{tr} are perfectly equal in both curves. In this case, the simulated a homogeneous medium with low absorption and very high scattering, where the DA is known to work better

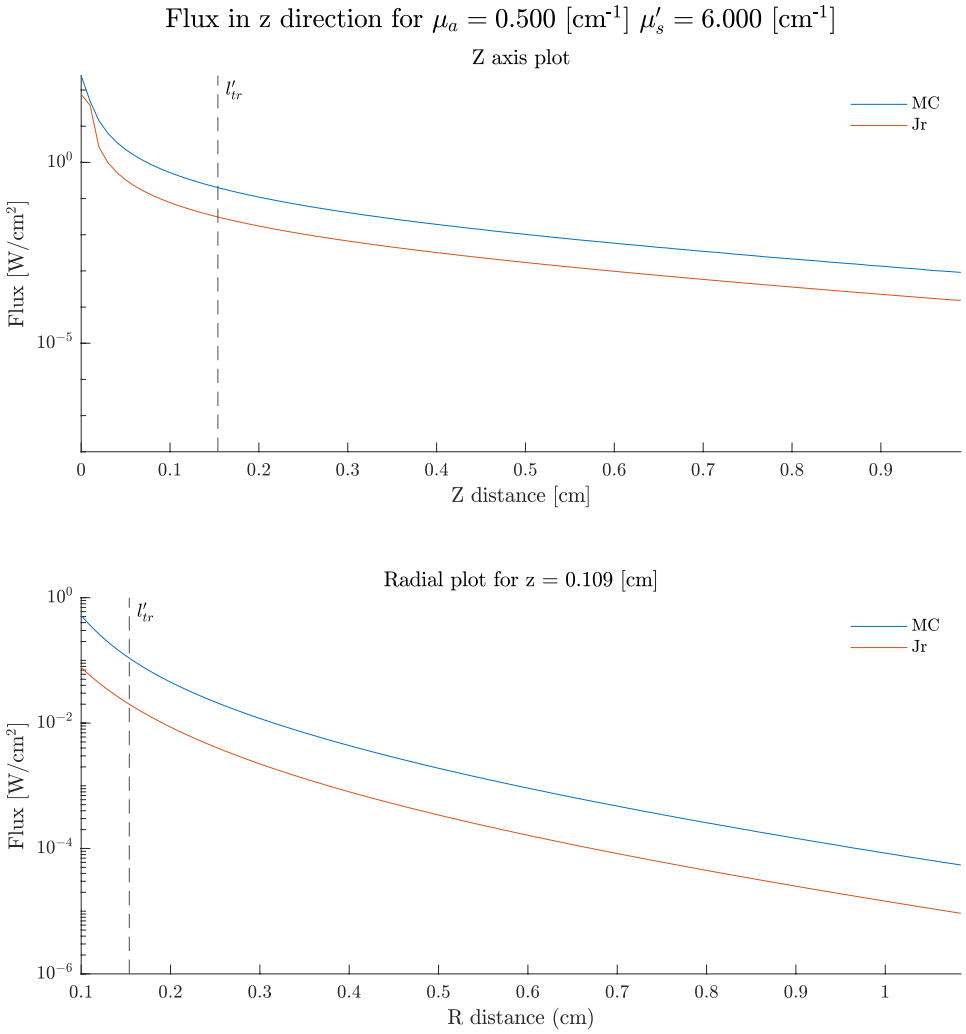

Figure 1.6 Comparison of the forward flux for a point source in a diffusive medium with optical properties $\mu_a = 0.5$ cm^{-1}, $\mu'_s = 6$ cm^{-1} and $g = 0.9$.

If the absorption is increased, we notice disagreements between the results of the MC and the analytic solution of $\mathbf{J}_d(\mathbf{r})$. This artifact can be seen in figure 1.7, where it can be observed that the flux Jr has a diverging trend respect to the MC solution. This is somehow

expected since a lot of discrepancy can be found in the literature discussing the expression of the diffusion coefficient in absorbing diffuse media. Some works have claimed that the standard definition of D (see equation **??**) has no validity in this regime [31–33]. This work propose new expressions to increase the accuracy of the DA in the presence of strong absorption. In this work, the expression derived in [34] and experimentally validated in [35] was used and compared respect to the conventional D, confirming that the DA still holds in absorbing media if this modification is used. In figure 1.7 the curve for Jr_{abs} shows much better agreement with the results from the DA. This result is of special relevance for imaging in the NIR since high water content tissues will present very high absorption rates. Moreover, it confirms that the expression derived in [34] is accurate.

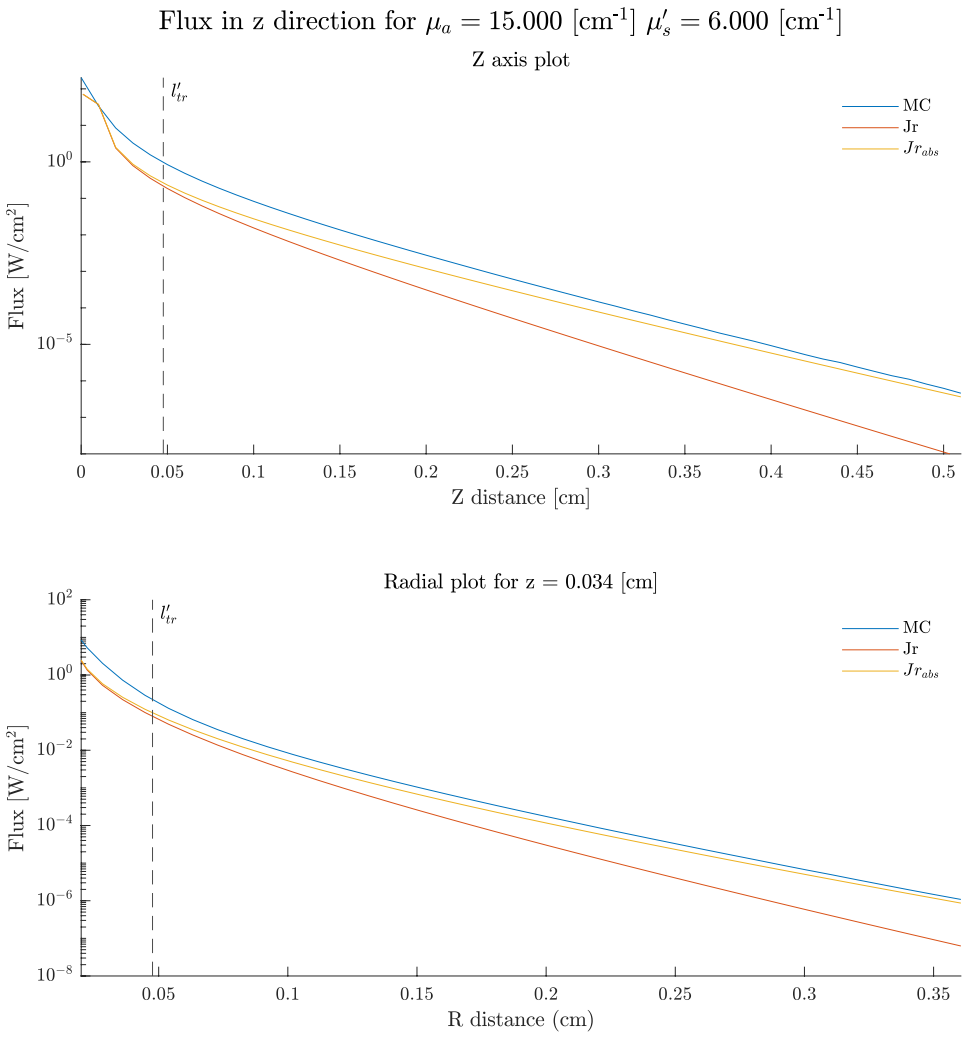

Figure 1.7 Comparison of the forward flux for a point source in an absorbing diffusive medium with optical properties μ_a = 15 cm^{-1}, μ_s' = 6 cm^{-1} and g = 0.9.

1.5 Monte Carlo Simulations of the Flux in Low Scattering Media

The results of the simulations of the flux for the point and the collimated beam sources in low scattering media are presented in this section, once that the MC implementation has been successfully validated.

1.5.1 Point Source

Simulations in low scattering media have been performed for μ_s' = 0.5 1/cm and μ_s' = 1 1/cm, both cases with low absorption. In both cases, the results show good agreement with the theory presented in this chapter. Figures 1.8 and 1.10 present plots in the z axis and in the radial direction for several l_{tr}^*. Figures 1.9 and 1.11 respresent the flux distributions in a 2D map.

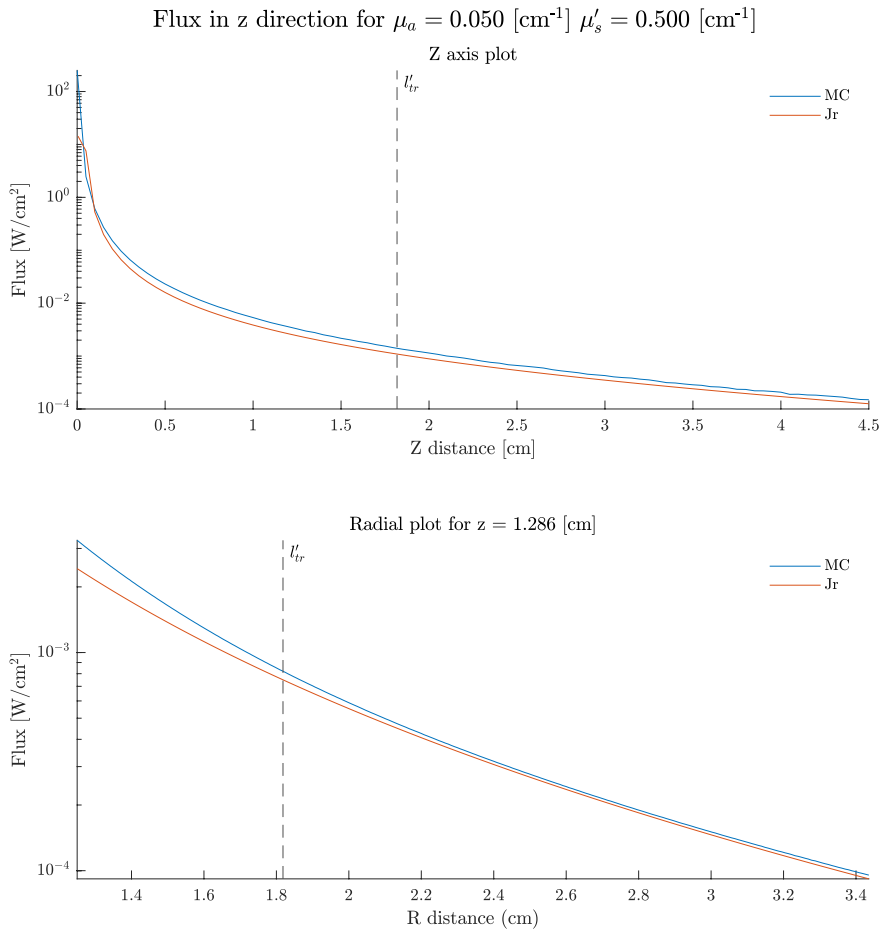

Figure 1.8 Comparison of the forward flux for a point source in a low scattering medium with optical properties μ_a = 0.5 cm^{-1}, μ_s' = 0.5 cm^{-1} and g = 0.9.

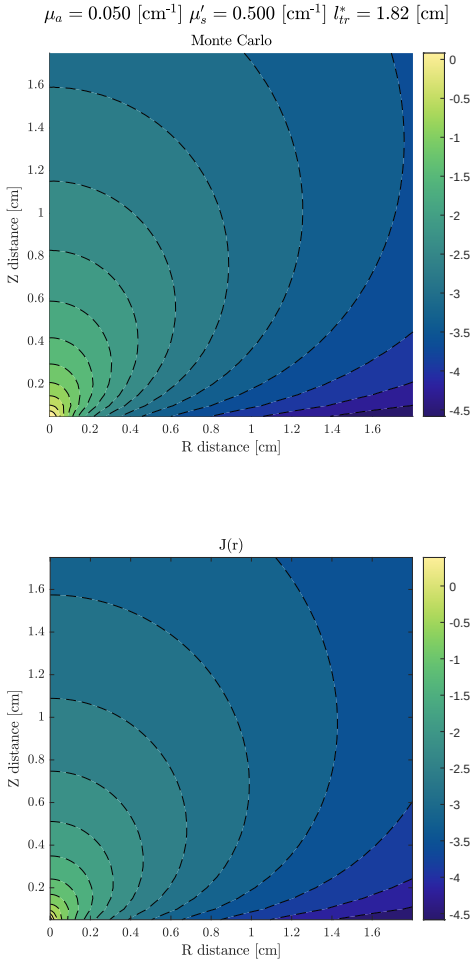

Figure 1.9 Comparison of the forward flux for a point source in a diffusive medium with optical properties μ_a = 0.5 cm^{-1}, μ_s' = 0.5 cm^{-1} and g = 0.9.

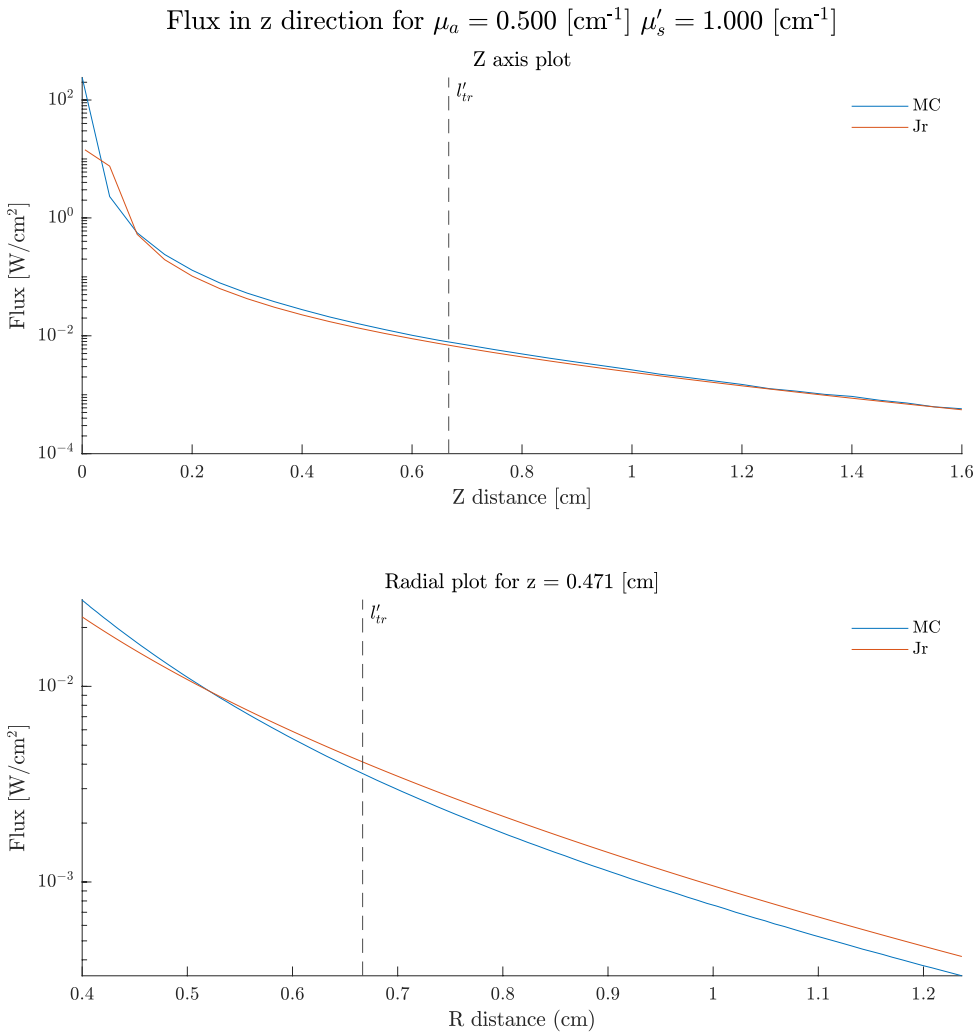

Figure 1.10 Comparison of the forward flux for a point source in a low scattering medium with optical properties μ_a = 0.5 cm^{-1}, μ_s' = 1 cm^{-1} and g = 0.9.

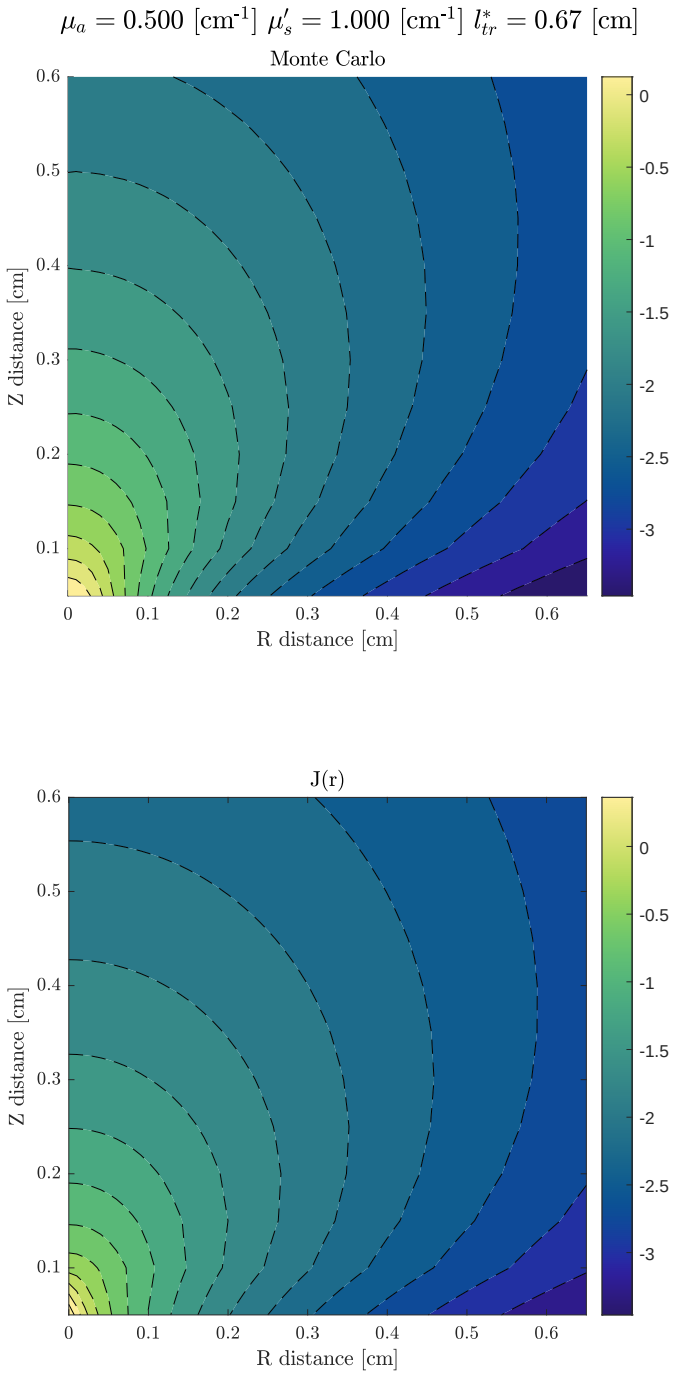

Figure 1.11 Comparison of the forward flux for a point source in a diffusive medium with optical properties μ_a = 0.5 cm^{-1}, μ_s' = 1 cm^{-1} and g = 0.9.

1.5.2 Collimated Pencil Beam Source

The case of the collimated source is more complex than the previous, since there are two well distinguished contributions with an intermediate transition between them. Figure 1.12 shows a simulation for a pencil source with optical properties μ_a = 1 1/cm and μ'_s = 1 1/cm compared with with the reduced and the diffuse flux components. A map of the pencil beam flux for the MC simulation is shown in figure 1.13.

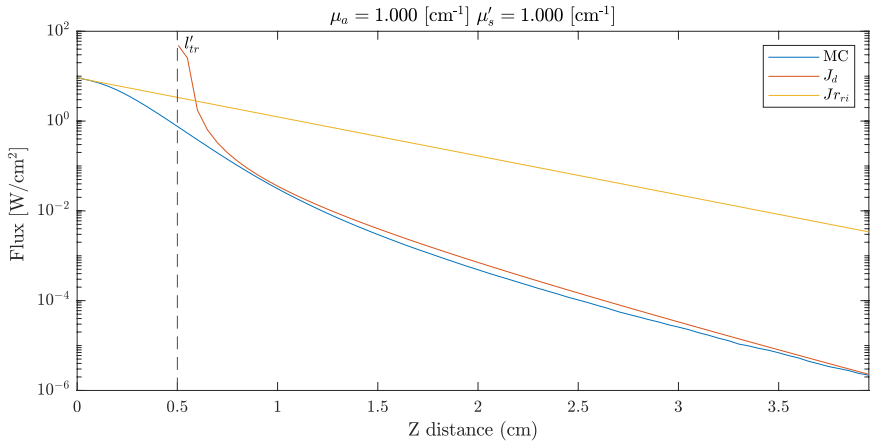

Figure 1.12 Comparison of the forward flux for a pencil source in a low scattering medium with optical properties μ_a = 1 cm^{-1}, μ'_s = 1 cm^{-1} and g = 0.9.

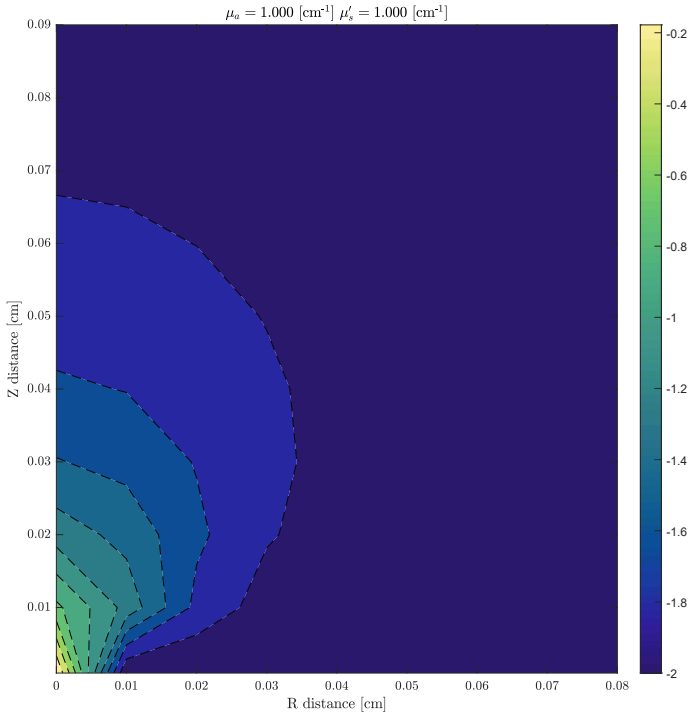

Figure 1.13 Flux for a point source in a low scattering medium with optical properties μ_a = 1 cm^{-1}, μ'_s = 1 cm^{-1} and g = 0.9.

1.6 Discussion

The results presented in the previous section showed good agreement with what was described by the theory, in fact, at far distances from the sources all the simulations there was a very good match in trends and magnitudes.

The point source simulations shown disagreements below the l^*_{tr} distance, which is predicted given the validity conditions of $U(\mathbf{r})$. In fact, both cases of scattering seem to have some degree of similarity in the trends of the mismatches, being the flux predicted by the MC simulation higher in both simulation cases. In the plots for the z axis, found in the top figure of figures 1.8 and 1.10, the values in the proximity to the source have stronger disagreement. It is important to comment here that this values are problematic for the analytic $\mathrm{J}(\mathbf{r})$, since it is calculated from the gradient of $U(\mathbf{r})$ and the Green's function has an asymptotic behaviour near 0. During the calculation of the curves for the analytic solution, as $U(\mathbf{r})$ cannot be evaluated at 0 we chose a value of 0.1 times $\mathrm{d}z$. The election of this value has a strong impact in the inital value of the gradient. If closer values to zero are used the gradient will also reflect the asymtotic nature of $U(\mathbf{r})$, therefore when interpreting the results this value simply cannot be trusted.

In the case of the simulations of the collimated pencil beam source, it can be seen that the trend shows two well distinguished propagation domains. Below l^*_{tr}, the MC simulation shows good agreement with the B-L in the first mm of propagation. Then, the flux slowly starts to decay to later fall into the diffusive regime. There are some important facts that should be pointed out here. The expression for the B-L flow, expressed as $\mathrm{J}_{ri}(\mathbf{r})$, is only defined along the propagation axis since it has a delta function in its expression. In cases with very low absorption like the one simulated here, the scattering events will quickly start to remove photons from the propagation axis, causing a quick decrease of the forward flux and increasing the photon flux in the adjacent bins. This is caused by the broadening of the beam towards z, which after a certain distance will lead into isotropic propagation of the photons. The broadening and loss of concetration of the flux in the central beam is depicted in figure 1.13.

If the diameter of the beam in these simulations were increased, the detected intensity in the central bin would match better to the B-L law, since the input can be approximated to a plane wave. However, in this case we would be not able to measure the changes in the diffuse flux since the measured flow would be constant. The results of these simulations manifest that even if a good B-L expression is found to model the decay along the propagation axis as in [36], the broadening of the beam that will drive the flux into diffusion is still unmodeled. Varying the diameter of the beam would be equivalent to changing the radial integration step of the simulator, actually this behaviour was observed during the tests of the simulator.

In the diffusion regime, the results match perfectly to the flux predicted by the theory, becoming equivalent to that of a point source located at l_{tr}^{*} attenuated the corresponding factor according to the B-L law.

References

[1] A. Ishimaru, *Wave Propagation and Scattering in Random Media*. Elsevier, 1978, p. 272. DOI: 10.1016/B978-0-12-374701-3.X5001-7.

[2] J. Ripoll, *Principles of Diffuse Light Propagation: Light Propagation in Tissues with Applications in Biology and Medicine*. World Scientific, 2012, p. 336. DOI: 10.1080/00107514.2013.810670.

[3] S. L. Jacques and B. W. Pogue, "Tutorial on diffuse light transport", *Journal of Biomedical Optics*, vol. 13, no. 4, p. 041 302, 2008. DOI: 10.1117/1.2967535.

[4] B. Chen, K. Stamnes, and J. J. Stamnes, "Validity of the diffusion approximation in bio-optical imaging", *Applied Optics*, vol. 40, no. 34, p. 6356, Dec. 2001. DOI: 10.1364/AO.40.006356.

[5] T. Spott and L. O. Svaasand, "Collimated light sources in the diffusion approximation", *Applied Optics*, vol. 39, no. 34, p. 6453, Dec. 2000. DOI: 10.1364/AO.39.006453.

[6] S. A. Prahl, "A Monte Carlo model of light propagation in tissue", in *Dosimetry of Laser Radiation in Medicine and Biology*, G. J. Mueller, D. H. Sliney, and R. F. Potter, Eds., vol. 10305, Jan. 1989, p. 1 030 509. DOI: 10.1117/12.2283590.

[7] K. M. Yoo, F. Liu, and R. R. Alfano, "When does the diffusion approximation fail to describe photon transport in random media?", *Physical Review Letters*, vol. 64, no. 22, pp. 2647–2650, May 1990. DOI: 10.1103/PhysRevLett.64.2647.

[8] Z. Q. Zhang, I. P. Jones, H. P. Schriemer, J. H. Page, D. A. Weitz, and P. Sheng, "Wave transport in random media: The ballistic to diffusive transition", *Physical Review E*, vol. 60, no. 4, pp. 4843–4850, Oct. 1999. DOI: 10.1103/PhysRevE.60.4843.

[9] I. Freund, M. Kaveh, and M. Rosenbluh, "Dynamic multiple scattering: Ballistic photons and the breakdown of the photon-diffusion approximation", *Physical Review Letters*, vol. 60, no. 12, pp. 1130–1133, 1988. DOI: 10.1103/PhysRevLett.60.1130.

[10] T. Tarvainen, M. Vauhkonen, V. Kolehmainen, S. R. Arridge, and J. P. Kaipio, "Coupled radiative transfer equation and diffusion approximation model for photon migration in turbid medium with low-scattering and non-scattering regions",

Physics in Medicine and Biology, vol. 50, no. 20, pp. 4913–4930, Oct. 2005. DOI: 10.1088/0031-9155/50/20/011.

[11] T. Hayashi, Y. Kashio, and E. Okada, "Hybrid Monte Carlo-diffusion method for light propagation in tissue with a low-scattering region", *Applied Optics*, vol. 42, no. 16, p. 2888, Jun. 2003. DOI: 10.1364/AO.42.002888.

[12] G. Mie, "Beiträge zur Optik trüber Medien, speziell kolloidaler Metallösungen", *Annalen der Physik*, vol. 330, no. 3, pp. 377–445, 1908. DOI: 10.1002/andp.19083300302.

[13] S. L. Jacques, "Optical properties of biological tissues: a review", *Physics in medicine and biology*, vol. 58, no. 11, pp. 37–61, Jun. 2013. DOI: 10.1088/0031-9155/58/11/R37.

[14] N. Bosschaart, G. J. Edelman, M. C. G. Aalders, T. G. van Leeuwen, and D. J. Faber, "A literature review and novel theoretical approach on the optical properties of whole blood", *Lasers in Medical Science*, vol. 29, no. 2, pp. 453–479, Mar. 2014. DOI: 10.1007/s10103-013-1446-7.

[15] A. N. Bashkatov, E. A. Genina, and V. V. Tuchin, "Optical properties of skin, subcutaneous, and muscle tissues: A review", *Journal of Innovative Optical Health Sciences*, vol. 04, no. 01, pp. 9–38, Jan. 2011. DOI: 10.1142/S1793545811001319.

[16] D. Zhu, J. Wang, Z. Zhi, X. Wen, and Q. Luo, "Imaging dermal blood flow through the intact rat skin with an optical clearing method", *Journal of Biomedical Optics*, vol. 15, no. 2, p. 026 008, 2010. DOI: 10.1117/1.3369739.

[17] D. S. Richardson and J. W. Lichtman, "Clarifying Tissue Clearing", *Cell*, vol. 162, no. 2, pp. 246–257, Jul. 2015. DOI: 10.1016/j.cell.2015.06.067.

[18] J. M. Hirshburg, "Chemical agent induced reduction of skin light scattering", PhD thesis, Texas A&M University, USA, 2009, p. 120, ISBN: 9781109679076.

[19] A. N. Bashkatov, K. V. Berezin, K. N. Dvoretskiy, M. L. Chernavina, E. A. Genina, V. D. Genin, and V. I. Kochubey, "Measurement of tissue optical properties in the context of tissue optical clearing", *Journal of Biomedical Optics*, vol. 23, no. 09, p. 1, Aug. 2018. DOI: 10.1117/1.JBO.23.9.091416.

[20] A. J. Moy, B. V. Capulong, R. B. Saager, M. P. Wiersma, P. C. Lo, A. J. Durkin, and B. Choi, "Optical properties of mouse brain tissue after optical clearing with FocusClear™", *Journal of Biomedical Optics*, vol. 20, no. 9, p. 095 010, Sep. 2015. DOI: 10.1117/1.JBO.20.9.095010.

[21] D. K. Tuchina, A. N. Bashkatov, E. A. Genina, and V. V. Tuchin, "Quantification of glucose and glycerol diffusion in myocardium", *Journal of Innovative Optical Health Sciences*, vol. 08, no. 03, p. 1 541 006, May 2015. DOI: 10.1142/S1793545815410060.

[22] H. Zhang, D. Salo, D. M. Kim, S. Komarov, Y.-C. Tai, and M. Y. Berezin, "Penetration depth of photons in biological tissues from hyperspectral imaging in shortwave

infrared in transmission and reflection geometries", *Journal of Biomedical Optics*, vol. 21, no. 12, p. 126 006, Dec. 2016. DOI: 10.1117/1.JBO.21.12.126006.

[23] M. Keijzer, S. L. Jacques, S. A. Prahl, and A. J. Welch, "Light distributions in artery tissue: Monte Carlo simulations for finite-diameter laser beams", *Lasers in Surgery and Medicine*, vol. 9, no. 2, pp. 148–154, 1989. DOI: 10.1002/lsm.1900090210.

[24] L. Wang, S. L. Jacques, and L. Zheng, "MCML—Monte Carlo modeling of light transport in multi-layered tissues", *Computer Methods and Programs in Biomedicine*, vol. 47, no. 2, pp. 131–146, Jul. 1995. DOI: 10.1016/0169-2607(95)01640-F.

[25] S. Staelens and I. Buvat, "Monte Carlo Simulations in Nuclear Medicine Imaging", in *Advances in Biomedical Engineering*, Elsevier, 2009, pp. 177–209. DOI: 10.1016/B978-0-444-53075-2.00005-8.

[26] X. Jia, X. Gu, Y. J. Graves, M. Folkerts, and S. B. Jiang, "GPU-based fast Monte Carlo simulation for radiotherapy dose calculation", *Physics in Medicine and Biology*, vol. 56, no. 22, pp. 7017–7031, Nov. 2011. DOI: 10.1088/0031-9155/56/22/002.

[27] A. Sisniega, W. Zbijewski, J. Xu, H. Dang, J. W. Stayman, J. Yorkston, N. Aygun, V. Koliatsos, and J. H. Siewerdsen, "High-fidelity artifact correction for cone-beam CT imaging of the brain", *Physics in Medicine and Biology*, vol. 60, no. 4, pp. 1415–1439, Feb. 2015. DOI: 10.1088/0031-9155/60/4/1415.

[28] E. Alerstam, T. Svensson, and S. Andersson-Engels, "Parallel computing with graphics processing units for high-speed Monte Carlo simulation of photon migration", *Journal of Biomedical Optics*, vol. 13, no. 6, p. 060 504, 2008. DOI: 10.1117/1.3041496.

[29] Q. Fang and D. A. Boas, "Monte Carlo Simulation of Photon Migration in 3D Turbid Media Accelerated by Graphics Processing Units", *Optics Express*, vol. 17, no. 22, p. 20 178, Oct. 2009. DOI: 10.1364/OE.17.020178.

[30] S. L. Jacques, "Light Distributions from Point, Line and Plane Sources for Photochemical Reactions and Fluorescence in Turbid Biological Tissues", *Photochemistry and Photobiology*, vol. 67, no. 1, pp. 23–32, Jan. 1998. DOI: 10.1111/j.1751-1097.1998.tb05161.x.

[31] R. Pierrat, J.-J. Greffet, and R. Carminati, "Photon diffusion coefficient in scattering and absorbing media", *Journal of the Optical Society of America A*, vol. 23, no. 5, p. 1106, May 2006. DOI: 10.1364/JOSAA.23.001106.

[32] R. Elaloufi, R. Carminati, and J.-J. Greffet, "Definition of the diffusion coefficient in scattering and absorbing media", *Journal of the Optical Society of America A*, vol. 20, no. 4, p. 678, Apr. 2003. DOI: 10.1364/JOSAA.20.000678.

[33] T. Durduran, A. G. Yodh, and B. Chance, "Does the photon-diffusion coefficient depend on absorption ?", *Journal of the Optical Society of America. A, Optics, image science, and vision*, vol. 14, no. 12, pp. 3358–3365, 1997. DOI: 10.1364/JOSAA.14.003358.

[34] R. Aronson and N. Corngold, "Photon diffusion coefficient in an absorbing medium", *Journal of the Optical Society of America A*, vol. 16, no. 5, p. 1066, May 1999. DOI: 10.1364/JOSAA.16.001066.

[35] J. Ripoll, D. Yessayan, G. Zacharakis, and V. Ntziachristos, "Experimental determination of photon propagation in highly absorbing and scattering media", *Journal of the Optical Society of America. A, Optics, image science, and vision*, vol. 22, no. 3, pp. 546–51, Mar. 2005. DOI: 10.1364/JOSAA.22.000546.

[36] I. Ben, Y. Y. Layosh, and E. Granot, "Study of a simple model for the transition between the ballistic and the diffusive regimes in diffusive media", *Journal of Biomedical Optics*, vol. 21, no. 6, p. 066 004, Jun. 2016. DOI: 10.1117/1.JBO.21.6.066004.